# JOURNAL PRE-PROOF

This is an early version of the article, published prior to copyediting, typesetting, and editorial correction. The manuscript has been accepted for publication and is now available online to ensure early dissemination, author visibility, and citation tracking prior to the formal issue publication.

It has not undergone final language verification, formatting, or technical editing by the journal's editorial team. Content is subject to change in the final Version of Record.

To differentiate this version, it is marked as "PRE-PROOF PUBLICATION" and should be cited with the provided DOI. A visible watermark on each page indicates its preliminary status.

The final version will appear in a regular issue of *Archives of Acoustics*, with final metadata, layout, and pagination.

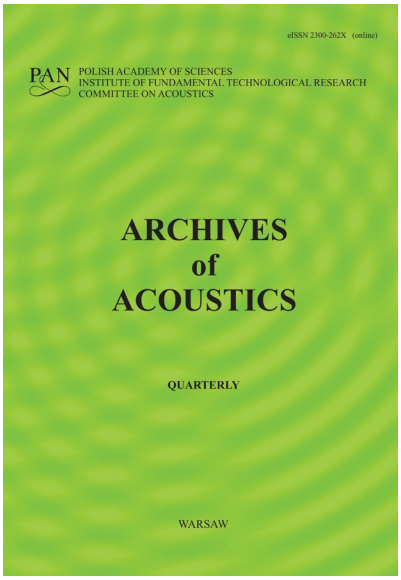


**Title:** Examination of low-frequency sound decay in two connected enclosed spaces having different sound absorption on boundary surfaces

**Author(s):** Mirosław Meissner

**DOI:** https://doi.org/10.24423/archacoust.2026.4443

**Journal:** *Archives of Acoustics*

**ISSN:** 0137-5075, e-ISSN: 2300-262X

**Publication status:** In press

**Received:** 2026-02-22

**Revised:** 2026-04-20

**Accepted:** 2026-04-27

**Published pre-proof:** 2026-04-30

**Please cite this article as:**

Meissner M. (2026), Examination of low-frequency sound decay in two connected enclosed spaces having different sound absorption on boundary surfaces, *Archives of Acoustics*, https://doi.org/10.24423/archacoust.2026.4443

# Examination of low-frequency sound decay in two connected enclosed spaces having different sound absorption on boundary surfaces

Mirosław Meissner

*Institute of Fundamental Technological Research, Polish Academy of Sciences*

*Pawińskiego 5B, 02–106 Warsaw, Poland*

e-mail: mmeissn@ippt.pan.pl, https://orcid.org/0000-0003-3885-0273



**Abstract**

In this paper, a sound decay in two connected enclosed spaces was investigated. The research concerned the low-frequency range, because in this situation the sound decay is predominantly non-exponential. Numerical simulations were performed for a system of two connected rectangular subrooms. The larger subroom was highly reverberant, while the smaller subroom had walls that provided moderate sound damping. Simulation results showed that after switching off the harmonic source, a non-exponential behavior of sound decay is usually observed. This is because many eigenmodes are involved in the sound decay, hence this process strongly depends on both the source frequency and its position. Reverberant properties of the system were also determined using energy decay curves calculated by the reverse-time integration of squared room impulse response. Simulations showed that the effect of the significant difference in sound absorption in subrooms is a wide range of modal reverberation time values, i.e. it is large for eigenmodes localized in a highly reverberant room and small for eigenmodes localized in a damped room. The analyzed room system is therefore characterized by an interesting feature resulting from the localization of eigenmodes. When the source is located in the larger subroom, slowly decaying modes localized in this subroom dominate the sound decay process. However, when the source is located in the smaller subroom, the sound decay in the larger subroom is much faster since non-localized modes with a shorter modal reverberation time are excited within this subroom.

**Key words:** coupled spaces, sound decay, sound absorption, room impulse response, decay times, localization of eigenmodes, modal reverberation time

## 1. Introduction

The phenomenon of sound decay inside enclosed spaces is of fundamental importance in room acoustics, as predicted decay times are the main quantities utilized to assess the room acoustic quality. Accurate determination of decay times is essential when evaluating the acoustics of concert halls (Ermann, Johnson, 2005; Bradley, Wang, 2007; Luizard *et al.*, 2015), irregularly shaped spaces such as churches (Martellotta, 2016; Girón, *et al.*, 2017; Sü Gül, 2021), and architectural structures in the form of connected enclosed spaces, also referred to as coupled spaces (Jasa, Xiang, 2009; Luizard, Katz, 2014a; Das, Abel, 2021). A special feature of coupled spaces is the possibility of achieving non-exponential sound decays (Bradley, Wang, 2009; Xiang *et al.*, 2011). This attribute is exploit in concert halls to obtain the double slope sound decay, characterized by a fast initial and a slow late decay, which listeners perceive as a beneficial balance between the reverberance and the sound clarity (Bradley, Wang, 2010).

A number of theoretical approaches and numerical implementations have been developed to investigate acoustical properties of coupled spaces. They utilize statistical-acoustic models, the diffusion-equation model, geometric methods, the improved Fourier series method and the modal analysis also known as the modal expansion method. Statistical-acoustic models (Summers *et al.*, 2004; Summers, 2012) are based on the diffuse sound field assumption, according to which sound energy is homogeneous in acoustic field and moves in all directions with the same probability. These hypotheses are roughly correct for sound frequencies above the Schroeder frequency (Schroeder, 1996). The diffusion-equation model (Xiang *et al.*, 2009; Luizard *et al.*, 2014; Sü Gül *et al.*, 2019) is an extension of the statistical theory to spatially changing reverberant sound fields and uses the analogy of the sound energy density with a density of "sound particles" travelling along straight lines. Geometrical methods are applicable at high sound frequencies, and most of the existing geometrical room acoustic modeling techniques are based on ray-tracing and beam tracking algorithms (Nijs *et al.*, 2002; Summers *et al.*, 2005). However, these methods do not allow all relevant propagation paths involving edge diffraction to be found. Therefore, the calculation results obtained by these methods may be inaccurate in the case of coupled spaces and irregularly shaped enclosures. The improved Fourier series method is used in studies of structural vibrations

and vibro-acoustic couplings, and has been successfully applied to the study of acoustics of two coupled spaces with a coupling opening of variable size (Shi *et al.*, 2005).

Wave phenomena in the sound field, such as diffraction and wave interferences, are fully described by modal analysis, but this method is more difficult to apply to enclosed spaces with irregular shapes. In this method, the response of an enclosure to sound excitation can be described by the modal expansion of the sound pressure and the decay coefficient associated with each acoustic mode (Meissner, 2010; Dance, Van Buuren, 2013). Modal analysis has proven to be particularly useful for systems of coupled spaces, as it enables the identification of phenomena such as the localization of eigenmodes (Meissner, 2009), the formation of acoustic energy vortices in the active sound intensity vector field (Meissner, 2012), and the occurrence of large dips in the spatial distribution of the sound pressure level under steady-state conditions (Meissner, Wiśniewski, 2019).

The objective of this paper is to examine the sound decay process in the system of two connected enclosed spaces with different sound absorption on boundary surfaces. The research focuses on the low-frequency range, since in this case a non-exponential nature of sound decay is usually observed. The theoretical model uses the modal expansion method, in which the reverberant sound pressure is decomposed into a series of eigenmodes with specific eigenfrequencies. The study takes into account two types of system responses. In the first case, a steady-state sound field is produced by a harmonic point source, and the sound decay process begins immediately after the source is switched off. In the second case, the system response is initiated by the point source emitting Dirac delta time impulse, and decay times are determined from a slope of energy decay curve calculated by the reverse-time integration of squared room impulse response. Numerical simulations were performed for a system of two connected rectangular rooms, where the larger room was highly reverberant and walls of the smaller room provided moderate sound damping.

## 2. Theoretical analysis

### *2.1. Problem definition*

The object of theoretical analysis is a system of two enclosed spaces $\Omega_1$ and $\Omega_2$ connected by a transparent opening (Fig. 1). The spaces are filled with air, hence the product $\rho c$

represents the impedance of air, where $\rho$ is the air density and $c$ is the sound speed. The sound pressure $p(\mathbf{r},t)$ in the system is generated by the volume sound source $q(\mathbf{r}',t)$, where $\mathbf{r}=(x,y,z)$ is a position of a field point and $\mathbf{r}'=(x',y',z')$ is a position of a source point.

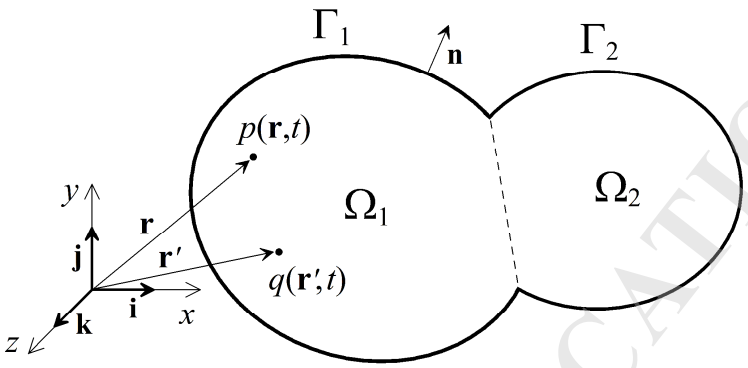


Figure 1: Analyzed system consisting of two enclosed spaces $\Omega_1$ and $\Omega_2$ connected by a transparent opening denoted by dashed line.

In general case, the time dependence of source function $q(\mathbf{r}',t)$ can be arbitrary, therefore the presented theory allows to determine the interior sound field in both the steady-state and reverberant conditions. A boundary surface of the system is marked by $\Gamma$ and it is divided in two parts $\Gamma_1$ and $\Gamma_2$ representing boundary surfaces of the spaces $\Omega_1$ and $\Omega_2$. It is assumed that the surfaces $\Gamma_1$ and $\Gamma_2$ are characterized by different sound absorption, therefore the sound pressure on these surfaces satisfies the following boundary conditions

$$\mathbf{r}\in\Gamma_i: \quad \boldsymbol{\nabla} p\cdot\mathbf{n}=-\frac{1}{cZ_i}\frac{\partial p}{\partial t}, \quad i=1,2, \tag{1}$$

where $\boldsymbol{\nabla}$ is the gradient operator, the dot is a scalar product, $\mathbf{n}$ is the outward normal vector, and $Z_i=|Z_i|e^{\mathrm{j}\phi_i}$ is the impedance on the surface $\Gamma_i$ normalized by the impedance of air. Due to random directions of incident sound waves, damping properties of the surface $\Gamma_i$ are determined by the random-incident absorption coefficient $\alpha_i$ given by (Paris, 1928)

$$\alpha_i=\frac{8\cos(\phi_i)}{|Z_i|^2}\left\{|Z_i|+\frac{\cos(2\phi_i)}{\sin(\phi_i)}\arctan\left[\frac{|Z_i|\sin(\phi_i)}{1+|Z_i|\cos(\phi_i)}\right]\right.$$
$$\left.-\ln\left[1+2|Z_i|\cos(\phi_i)+|Z_i|^2\right]\cos(\phi_i)\right\}. \tag{2}$$

Since it was assumed that the system is characterized by different sound absorption on the boundary surfaces $\Gamma_1$ and $\Gamma_2$, from theoretical and practical points of view, the case when the

absorption coefficients $\alpha_1$ and $\alpha_2$ differ significantly deserves careful analysis. The research focuses on the low-frequency range, since in this case the sound decay strongly depends on the excitation frequency. At low frequencies, typical absorptive materials provide a small sound damping, so the system under consideration can be treated as lightly damped.

### *2.2. Low-frequency sound decay*

At low frequencies, a physically correct description and interpretation of acoustics in enclosed spaces requires a use of wave-based methods. This is particularly necessary when simulating sound decay in enclosures with irregular shapes and systems of coupled rooms, because in such cases the theoretical model should take sound diffraction into account. In room acoustics, the most convenient way to describe a low-frequency sound field is to use the room impulse response (RIR). This is because a knowledge of the RIR function $h(\mathbf{r}', \mathbf{r}, t)$, which describes the pressure response at the receiving point $\mathbf{r} = (x, y, z)$ to the time impulse generated at the source point $\mathbf{r}' = (x', y', z')$, makes it possible to determine the response of a room to any sound excitation. When the spatial and temporal properties of the source function $q(\mathbf{r}', t)$ are known, the pressure response to this excitation can be determined using the convolution integral in the time domain (Damelin, Miller, 2012)

$$p(\mathbf{r}, t) = \int_V q(\mathbf{r}', t) * h(\mathbf{r}', \mathbf{r}, t)\, \mathrm{d}^3\mathbf{r}' = \int_{-\infty}^{t} \int_V q(\mathbf{r}', \tau) h(\mathbf{r}', \mathbf{r}, t-\tau)\, \mathrm{d}^3\mathbf{r}' \mathrm{d}\tau, \tag{3}$$

where $V$ is the volume of a room system, the asterisk denotes a convolution operation and $\mathrm{d}^3\mathbf{r}' = \mathrm{d}x'\,\mathrm{d}y'\,\mathrm{d}z'$ is the volume element. A method for finding the RIR function was presented by Meissner and Wiśniewski (2020) and the result obtained is as follows

$$h(\mathbf{r}', \mathbf{r}, t) = c^2 \sum_{m=1}^{\infty} \frac{e^{-\xi_m t} \sin(\psi_m t) \Phi_m(\mathbf{r}') \Phi_m(\mathbf{r})}{\psi_m}, \tag{4}$$

where $m$ is a mode number, $\Phi_m$ are eigenfunctions, which fulfill the orthonormal property in the volume $V$, the damping coefficients $\xi_m$ are computed from the equation

$$\xi_m = r_m + \mathrm{j}\varphi_m = \frac{c}{2} \left[ \int_{\Gamma_1} \frac{\Phi_m^2(\mathbf{r}_s) \mathrm{d}\Gamma}{Z_1} + \int_{\Gamma_2} \frac{\Phi_m^2(\mathbf{r}_s) \mathrm{d}\Gamma}{Z_2} \right], \tag{5}$$

where $\mathbf{r}_s$ is the coordinate of the position on boundary surfaces $\Gamma_1$ and $\Gamma_2$, $\mathrm{j} = (-1)^{1/2}$ is the

imaginary unit, $\psi_m$ are complex frequencies determined from the formula

$$\psi_m = \Omega_m + \mathrm{j}\vartheta_m = \sqrt{\frac{a_m + \sqrt{a_m^2 + b_m^2}}{2}} + \mathrm{j}\sqrt{\frac{-a_m + \sqrt{a_m^2 + b_m^2}}{2}}, \tag{6}$$

where $a_m = \omega_m^2 - r_m^2 + \varphi_m^2$, $b_m = -2r_m\varphi_m$, and $\omega_m$ are eigenfrequencies, which are related to the corresponding eigenfunctions $\Phi_m$ through the equations

$$\Delta\Phi_m + \left(\frac{\omega_m}{c}\right)^2 \Phi_m = 0, \tag{7}$$

where $\Delta = \boldsymbol{\nabla}\cdot\boldsymbol{\nabla}$ is the Laplace operator.

Two methods are mainly used to describe the process of sound decay inside room systems. In the first method, the sound decay process is analyzed in the case of switching off the harmonic point source that created the steady-state sound field inside a room system. Therefore, in this case, the source function in Eq. (3) assumes the form

$$q(\mathbf{r}', \tau) = Q\delta(\mathbf{r}' - \mathbf{r}_0)e^{\mathrm{j}\omega\tau}, \tag{8}$$

where $Q = (8\pi\rho cW)^{1/2}$, $W$ is the source power (Kinsler *et al.*, 2000), $\omega$ is the source angular frequency and $\mathbf{r}_0 = (x_0, y_0, z_0)$ determines the source position. From a theoretical point of view, the steady-state sound field is achieved when the time interval between the present time $\tau$ and the moment of activation of the source is infinitely long. Therefore, in Eq. (3), it should be assumed that the source was turned on at the moment $\tau = -\infty$. Furthermore, to simplify the analysis, it is assumed that the source is stopped at the moment $\tau = 0$, hence after substituting Eq. (8) into Eq. (3) and performing integration we obtain the formula

$$p(\mathbf{r}, t) = c^2 Q \sum_{m=1}^{\infty} \frac{e^{-\xi_m t}\,\Phi_m(\mathbf{r}_0)\Phi_m(\mathbf{r})}{\omega_m^2 - \omega^2 + 2\mathrm{j}\omega\xi_m} \left[\cos(\psi_m t) + \frac{(\xi_m + \mathrm{j}\omega)\sin(\psi_m t)}{\psi_m}\right] \tag{9}$$

describing sound decay after switching off a harmonic point source. A quantity often used to evaluate this decay is the modal reverberation time $T_m$, defined as the time required for the pressure level to decay by 60 dB in the mth mode, so

$$T_m = \frac{3\ln(10)}{r_m}, \tag{10}$$

where the damping coefficient $r_m$, which is the real part of $\xi_m$, can be calculated from Eq. (5). Using Eq. (9), the spatial distribution of the pressure amplitude can be determined

for different times $t$, which allows us to predict changes in this distribution as time increases. Furthermore, at a given position $\mathbf{r}$ of the field, Eq. (9) allows one to calculate the changes in pressure amplitude over time in order to illustrate the nature of sound decay and, if possible, to estimate decay times.

The most commonly used method for analyzing sound decay in enclosed spaces is the method based on the reverse-time integration of the squared RIR (Schroeder, 1995). This method produces a smoothed decay profile, commonly known as the energy decay curve (EDC), which is used to estimate decay times. Assuming that a time impulse is emitted by a source located at the point $\mathbf{r}_0$ and transforming the right-hand side of Eq. (4), we obtain

$$h(\mathbf{r}_0, \mathbf{r}, t) = \sum_{m=1}^{\infty} \left[\alpha_m(t) + \mathrm{j}\beta_m(t)\right] \Phi_m(\mathbf{r}_0)\Phi_m(\mathbf{r}), \tag{11}$$

where $\alpha_m(t)$ and $\beta_m(t)$ can be determined from the equations

$$\begin{aligned}\alpha_m(t) = \frac{c^2 e^{-r_m t}}{\Omega_m^2 + \vartheta_m^2}\Big\{&\left[\Omega_m \sin(\varphi_m t) + \vartheta_m \cos(\varphi_m t)\right]\cos(\Omega_m t)\sinh(\vartheta_m t)\\ &+ \left[\Omega_m \cos(\varphi_m t) - \vartheta_m \sin(\varphi_m t)\right]\sin(\Omega_m t)\cosh(\vartheta_m t)\Big\},\end{aligned} \tag{12}$$

$$\begin{aligned}\beta_m(t) = \frac{c^2 e^{-r_m t}}{\Omega_m^2 + \vartheta_m^2}\Big\{&\left[\Omega_m \cos(\varphi_m t) - \vartheta_m \sin(\varphi_m t)\right]\cos(\Omega_m t)\sinh(\vartheta_m t)\\ &- \left[\Omega_m \sin(\varphi_m t) + \vartheta_m \cos(\varphi_m t)\right]\sin(\Omega_m t)\cosh(\vartheta_m t)\Big\}.\end{aligned} \tag{13}$$

As can be seen from Eq. (11), the RIR function takes complex values, so the quantity corresponding to the squared RIR is the square of the modulus of $h(\mathbf{r}_0, \mathbf{r}, t)$

$$|h(\mathbf{r}_0, \mathbf{r}, t)|^2 = \left[\sum_{m=1}^{\infty} \alpha_m(t)\,\Phi_m(\mathbf{r}_0)\Phi_m(\mathbf{r})\right]^2 + \left[\sum_{m=1}^{\infty} \beta_m(t)\,\Phi_m(\mathbf{r}_0)\Phi_m(\mathbf{r})\right]^2, \tag{14}$$

thus, EDC can be calculated using the reverse-time integration

$$\mathrm{EDC}(t) = \int_t^{\infty} |h(\mathbf{r}_0, \mathbf{r}, \tau)|^2 \,\mathrm{d}\tau. \tag{15}$$

A decibel version of EDC, here denoted by $L_{\mathrm{EDC}}$, can be determined from the formula

$$L_{\mathrm{EDC}}(t) = 10 \log\left[\frac{\mathrm{EDC}(t)}{\mathrm{EDC}(0)}\right], \tag{16}$$

and based on the slope of $L_{\mathrm{EDC}}$ at different stages of the sound decay process, the corresponding decay times can be predicted.

## 3. Numerical study

### *3.1. System of coupled spaces under consideration*

A process of sound decay was numerically tested for the system of two connected rectangular subrooms of the same height. The choice of the research object was dictated by practical considerations, as buildings and public facilities often contain spaces in the form of two-room coupled systems. This system together with the associated coordinate system is depicted in Fig. 2. Therefore, the wall areas of subrooms A and B are as follows

$$S_1 = 2(d_1 + h)l_1 + (d_1 + 2d_2)h, \tag{17}$$

$$S_2 = 2(d_3 + h)l_2 + d_3 h. \tag{18}$$

In the numerical study, the following dimensions of the room system were assumed: $l_1 = 15$ m, $l_2 = 5$ m, $d_1 = 10$ m, $d_2 = 2$ m, $d_3 = 6$ m and $h = 4$ m.

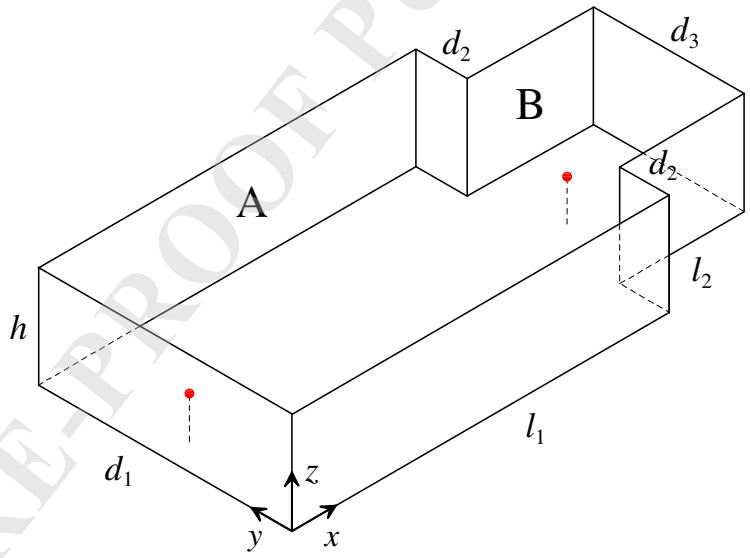


Figure 2: Room system under investigation containing two connected rectangular rooms marked with letters A and B. Red dots indicate locations of the sound source.

As shown by the theoretical analysis, the RIR function (Eq. (4)) and the reverberant sound field (Eq. (9)) are dependent on the sound source position. Therefore, in computer simulations it was assumed that the source is placed either at the point $\mathbf{r}_0 = (2\,\mathrm{m}, 4\,\mathrm{m}, 1.6\,\mathrm{m})$ or at the point $\mathbf{r}_0 = (17\,\mathrm{m}, 4\,\mathrm{m}, 1.6\,\mathrm{m})$ located inside subrooms A and B, respectively (Fig. 2).

The reverberant sound field distribution and decay times were determined on a horizontal plane located 1.2 m above the floor.

Since a characteristic feature of the analyzed room system is a different sound absorption on boundary surfaces, it was assumed that subroom A has almost acoustically hard walls, whose absorption properties can be described by the real-valued surface impedance (Thydal *at al.*, 2021). Therefore, the surface impedance $Z_1$ was assumed to have the value of 250, and using Eq. (2), it can be calculated that this value corresponds the absorption coefficient $\alpha_1$ of 0.031. On the other hand, it was assumed that subroom B is moderately damped, because the surface of its walls has the impedance $Z_2 = 10e^{\mathrm{j}\pi/6}$, for which the absorption coefficient $\alpha_2$ is 0.44. The absorption coefficient characterizing a sound damping in the whole room system is defined as (Vorländer, 2020)

$$\bar{\alpha} = \frac{\alpha_1 S_1 + \alpha_2 S_2}{S_1 + S_2}, \tag{19}$$

so, using Eqs. (17)–(19), it can be found that $\bar{\alpha} = 0.12$, which is a value low enough to treat the considered room system as lightly damped.

According to the wave theory, in the low-frequency range enclosed spaces may be treated as acoustic resonators with characteristic modes determined by the eigenfunctions $\Phi_m$ and eigenfrequencies $\omega_m$. Since the analyzed room system has a complex geometry, it is not possible to determine the functions $\Phi_m$ analytically, so numerical methods must be used. However, the fact, that the system under consideration is lightly damped allows the functions $\Phi_m$ to be approximated by the eigenfunctions determined for the rigid walls. Thus, in this case $\Phi_m$ can be described using the functions in the form (Kuttruff, 2017)

$$\Phi_m(\mathbf{r}) = \Psi_\kappa(x, y)\, \Theta_\mu \cos\left(\frac{\pi \mu z}{h}\right), \tag{20}$$

where the modal numbers $\kappa, \mu = 0, 1, 2\ldots$ are not simultaneously equal to zero, the eigenfunctions $\Psi_\kappa$ satisfy the orthonormal property over the surface $S$ of a horizontal cross-section of the system, $\Theta_\mu = 1/\sqrt{h}$ for $\mu = 0$ and $\Theta_\mu = \sqrt{2/h}$ for $\mu > 0$. Finally, the formula for calculating the frequency of the $m$th mode is given by

$$f_m = \sqrt{f_\kappa^2 + \left(\frac{\mu c}{2h}\right)^2}, \tag{21}$$

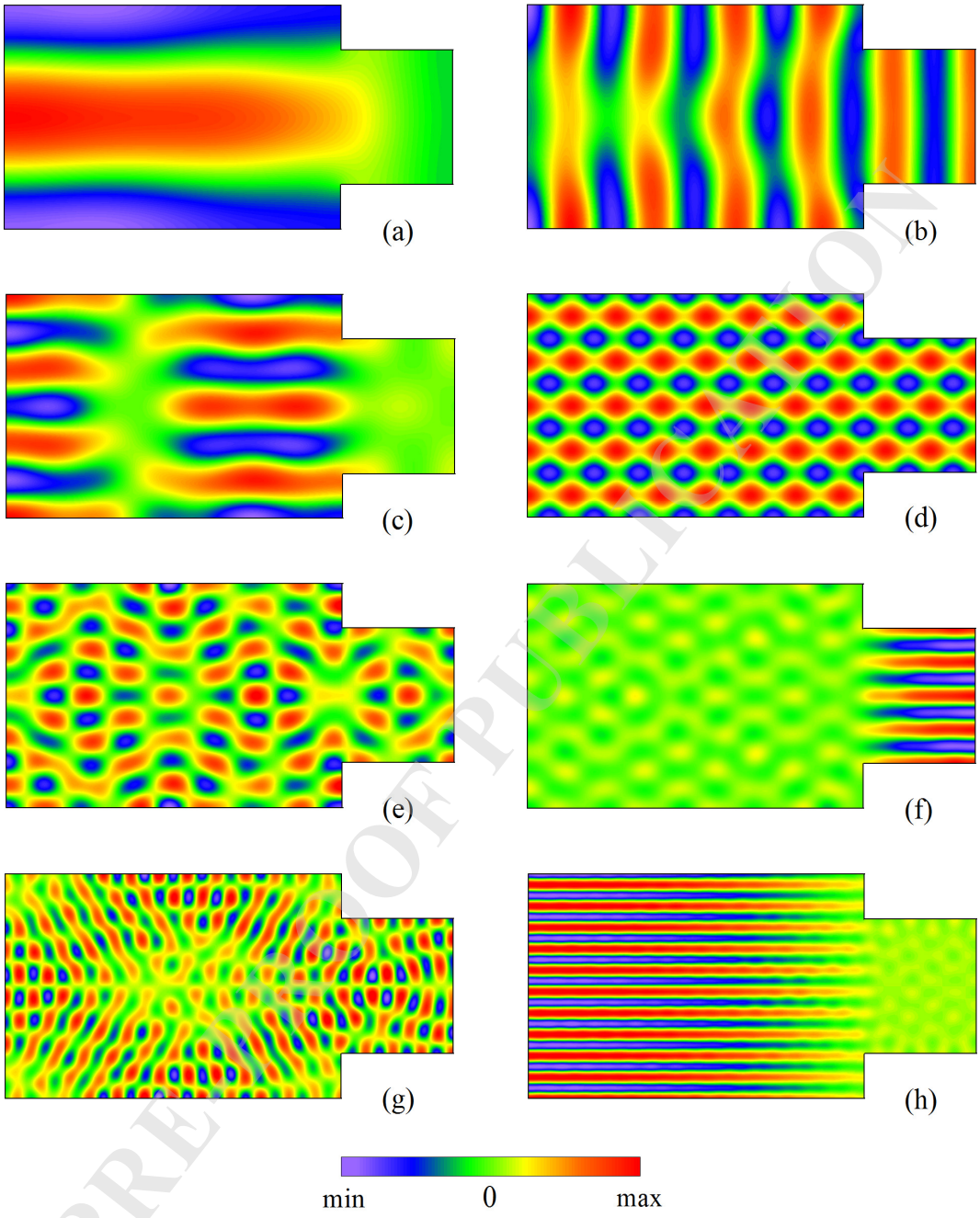


Figure 3: Contour maps of eigenfunctions $\Psi_\kappa$ for the modal number $\kappa$: (a) 9, (b) 50, (c) 60, (d) 154, (e) 200, (f) 271, (g) 500, (h) 652. Frequencies $f_\kappa$ for these functions are (in Hz): (a) 34.5, (b) 93.4, (c) 104, (d) 171.5, (e) 195.1, (f) 229.2, (g) 313.9, (h) 360.2.

where the eigenfrequencies $f_\kappa$ are associated with the functions $\Psi_\kappa$, and since $\Psi_0 = 1/\sqrt{S}$, the eigenfrequency $f_\kappa$ for $\kappa = 0$ is equal to zero.

Using the finite element method, the eigenfunctions $\Psi_\kappa$ were calculated for the first 5450 $m$-indexed eigenmodes with the frequencies $f_m$ up to 400 Hz. Examples of contour maps of the eigenfunctions $\Psi_\kappa$ with corresponding modal frequencies $f_\kappa$ are shown in Fig. 3. These results indicate that for some modes the acoustic energy may be concentrated within one of the subrooms (Figs. 3(a)(c)(f)(h)). This phenomenon is called the localization of eigenmodes and occurs in enclosed spaces of irregular shape. It should be emphasized that among modes calculated for the analyzed room system, there are also modes which are totally delocalized. This is because they represent modes of a cuboidal space with height $h$ and the width $d_1$, like the system under study, and length being the sum of $l_1$ and $l_2$ (Fig. 2). The contour map of the eigenfunction $\Psi_\kappa$ for such a mode is shown in Fig. 3(d).

### *3.2. Analysis of sound decay after turning off harmonic source*

As shown in Subsection 2.2, the theoretical model allows for determining the spatial distribution of the pressure amplitude after the harmonic source is turned off. In this case, as indicated by Eq. (9), the sound pressure $p(\mathbf{r}, t)$ is the sum of decaying modal oscillations. From this it follows that the amplitude of this pressure depends on time, therefore, to determine this amplitude, the discrete Hilbert transform $H_d$ was used, in which the pressure signal was represented by $p_r(\mathbf{r}, n)$, $n = 0, 1, ..., N-1$, i.e., the digitally sampled real part of $p(\mathbf{r}, t)$. Thus, the formula for calculating the pressure amplitude is as follows

$$P(\mathbf{r}, n) = \sqrt{p_r^2(\mathbf{r}, n) + H_d^2\{p_r(\mathbf{r}, n)\}}, \tag{22}$$

where the discrete Hilbert transform of $p_r(\mathbf{r}, n)$ is determined by (Kak, 1970)

$$H_d\{p_r(\mathbf{r}, n)\} = \begin{cases} \dfrac{2}{\pi} \displaystyle\sum_{m=\text{odd}}^{N-1} \dfrac{p_r(\mathbf{r}, n)}{n-m}, & n \text{ even}, \\ \dfrac{2}{\pi} \displaystyle\sum_{m=\text{even}}^{N-1} \dfrac{p_r(\mathbf{r}, n)}{n-m}, & n \text{ odd}. \end{cases} \tag{23}$$

In the numerical study, the distributions of pressure amplitude $P$ on the observation plane were computed for selected source frequencies and different times $t$ from the moment of switching off the source ($t = 0$). Furthermore, in order to illustrate the character of sound decay, the changes in sound pressure $p_r$ and pressure level $L_w$ over time at the receiving

point $\mathbf{r} = (8\,\mathrm{m}, 7\,\mathrm{m}, 1.2\,\mathrm{m})$ located on the observation plane were calculated. The formula used to determine the pressure level $L_w$ was as follows

$$L_w = 20 \log \left( \frac{P}{P_{\max}} \right), \tag{24}$$

where $P_{\max}$ is a maximum of $P$ recorded for the time $t$ greater than or equal to zero. Colored contour maps in Fig. 4 illustrate distributions of $P$ on the observation plane in the case when the harmonic source is located in subroom A. They were obtained for frequencies of 104 Hz and 257 Hz and times $t$ of 0 s, 2 s and 4 s. These data show that after turning off the source, it takes as long as 4 seconds for the pressure amplitude level to drop by approximately 36 dB for the first frequency and by 47 dB for the second frequency. This nature of the sound decay is obviously due to the fact that subroom A has walls that are almost acoustically hard.

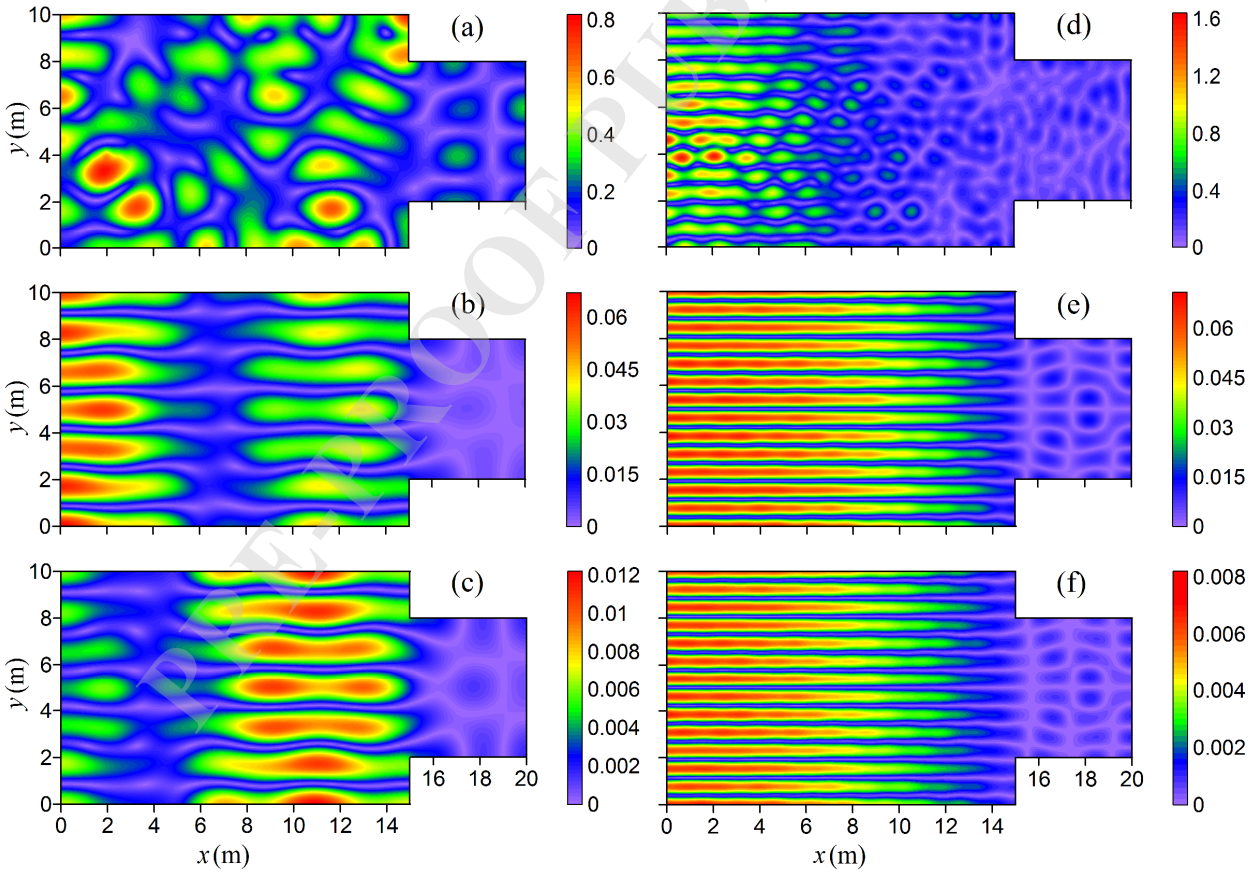


Figure 4: Changes in the pressure amplitude $P$ (in pascals) on observation plane for excitation frequency: (a)–(c) 104 Hz, (d)–(f) 257 Hz, and the time $t$: (a), (d) 0 s, (b), (e) 2 s, (c), (f) 4 s. Sound source located in subroom A.

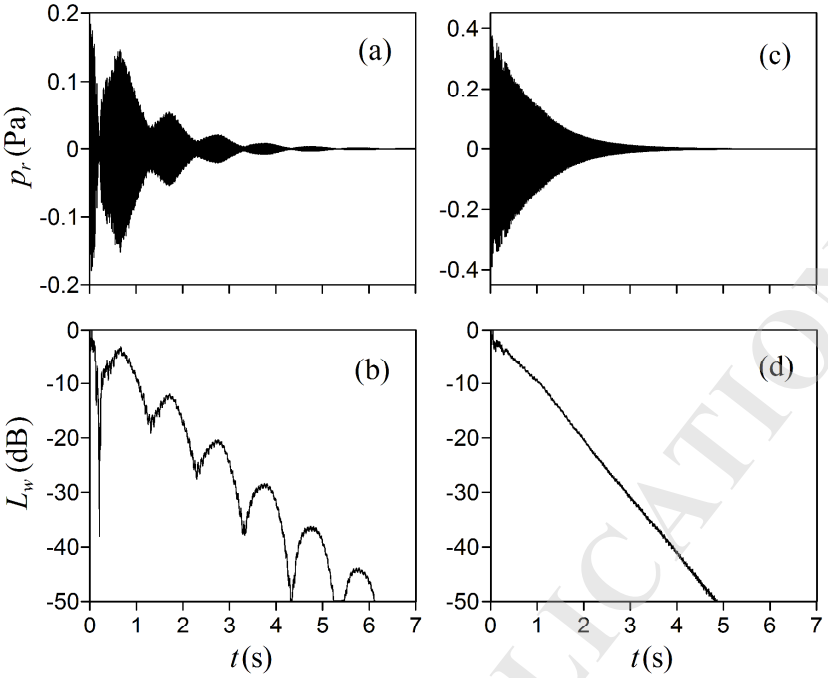


Figure 5: Variations in of the sound pressure $p_r$ and the pressure level $L_w$ at receiving point for excitation frequency: (a),(b) 104 Hz, (c),(d) 257 Hz. Sound source located in subroom A.

As may be seen from Fig. 4, the distributions of $P$ on the observation plane may change as time $t$ increases (Figs. 4(a)–(c)), or after a certain moment, a further increase in $t$ does not affect these distributions (Fig. 4(d)–(f)). The first situation occurs when strongly excited eigenmodes have eigenfrequencies very close to the source frequency, while the second one occurs when, after some time, the sound decay becomes almost perfectly exponential. The explanation of these finding can be found in Fig. 5, which depicts variations in the sound pressure $p_r$ and the pressure level $L_w$ at the receiving point for the frequencies considered. As can be seen in Figs. 5(a) and 5(b), for an excitation frequency of 104 Hz, the acoustic signal recorded at the receiving point has a form of decaying beating oscillations, and these beats are so large that the pressure level $L_w$ reaches its maximum value after 0.6 seconds from the moment the source is turned off. Detailed analysis of the numerical data allowed us to conclude that two eigenmodes with the modal number $m$ of 130 and 134, having frequencies of 103.03 Hz and 103.99 Hz, are responsible for the strong beating effect. The shape of the eigenfunction $\Psi_\kappa$ for the 134th eigenmode is shown in Fig. 3(c). Since these eigenmodes are localized in subroom A, the modal reverberation times determined for these

modes from Eq. (10) have large values, i.e. 6.19 s for the 130th eigenmode and 5.14 s for 134th eigenmode.

In the case of the excitation frequency of 257 Hz, the nature of the sound decay is different, because after a certain time has elapsed since the sound source was turned off, the acoustic response of the room system is dominated by one eigenmode. As a consequence, beyond this time, the observed temporal changes in the pressure level $L_w$ for this eigenmode are almost perfectly linear (Fig. 5(d)). As it results from Figs. 4(e) and 4(f), this eigenmode is localized in subroom A and based on the analysis of numerical data it was recognized as the 1544th eigenmode. The modal reverberation time for this mode is 5.87 s and this result agrees very well with a decay time of 5.85 s predicted from changes in the pressure level $L_w$ for time above 2 s.

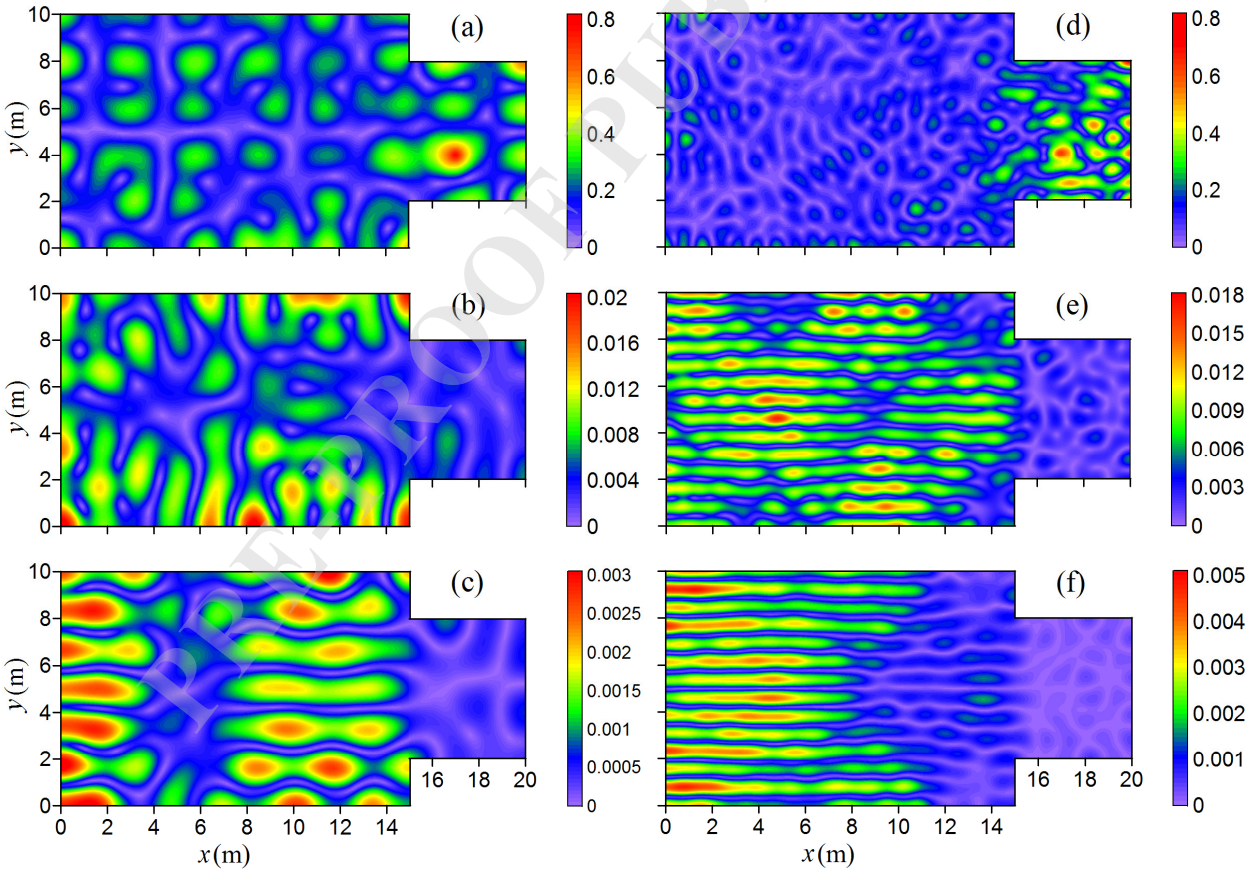


Figure 6: Changes in the pressure amplitude $P$ (in pascals) on observation plane for excitation frequency: (a)–(c) 104 Hz, (d)–(f) 257 Hz, and the time $t$: (a), (d) 0 s, (b), (e) 1 s, (c), (f) 2 s. Sound source located in subroom B.

In the next part of the numerical study, the influence of changing the sound source position on the sound decay process was investigated. The calculation results presented in Fig. 6 show changes in the pressure amplitude $P$ on the observation plane simulated for the same excitation frequencies as before and the times $t$ of 0 s, 1 s and 2 s in the case when the sound source is located in subroom B. From the comparison of Figs. 4 and 6 it follows that there is a qualitative similarity of pressure distributions some time after the sound source is turned off, caused by the influence of slowly decaying modes localized in subroom A on the sound decay. However, this comparison also indicates significant differences in the sound decay process, because the data in Fig. 6 show that for a frequency of 104 Hz the sound level drops by as much as 47 dB just 2 seconds after the source is turned off, and by 43 dB for a frequency of 257 Hz. This means that moving the source from subroom A to the subroom B results in a faster initial decay and a slower late decay. This conclusion is confirmed by the calculation results shown in Fig. 7, illustrating variations in the sound pressure $p_r$ and the pressure level $L_w$ at receiving point for the frequencies considered in the case when the sound source is located in subroom B.

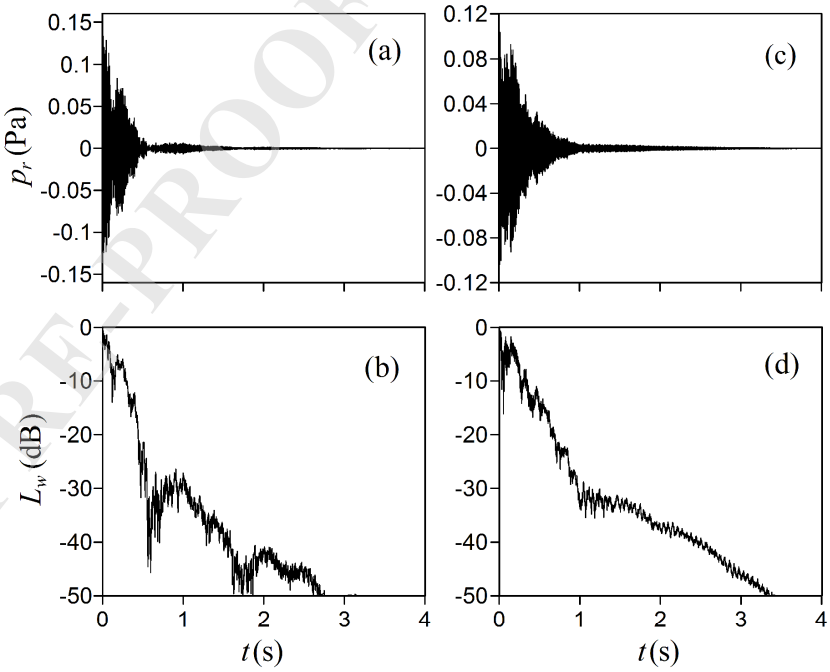


Figure 7: Variations in the sound pressure $p_r$ and the pressure level $L_w$ at receiving point for excitation frequency: (a),(b) 104 Hz, (c),(d) 257 Hz. Sound source located in subroom B.

The above analysis clearly shows that in the considered system of coupled spaces, the sound decay process after turning off harmonic source is extremely complex. This results not only from the fact that this process is strongly dependent on frequency, but, as shown in Eq. (9) and the obtained calculation results, its nature is also significantly influenced by the location of the sound source. Another phenomenon that has a major impact on sound decay is the localization of eigenmodes, and when the eigenmode localized in a subroom with very low sound damping dominates this process, a long-term exponential sound decay can be observed. Apart from this special case, the decay of the sound behaves very irregularly due to the excitation of eigenmodes with very similar modal frequencies, resulting in a beating effect, or the excitation of eigenmodes characterized by different modal decay times.

### *3.3. Results of decay times prediction from variations of $L_{\mathrm{EDC}}$*

As stated in Subsection 2.2, the method based on the reverse-time integration of the squared RIR is a procedure often employed to analyze the sound decay in enclosed spaces. Using Eq. (16), $L_{\mathrm{EDC}}$, the decibel version of EDC, was determined and the application of linear regression to relevant parts of $L_{\mathrm{EDC}}$ enabled the prediction of the early decay time (EDT), the decay times $T_{10}$, $T_{20}$, $T_{30}$ and the late decay time (LDT). EDT is the decay time evaluated from a decrease in $L_{\mathrm{EDC}}$ from 0 to $-10$ dB, multiplied by a factor of 6. $T_{10}$ is defined as the decay time estimated from a drop of $L_{\mathrm{EDC}}$ from $-5$ to $-15$ dB, multiplied by a factor of 6. $T_{20}$ is defined as the decay time estimated from a drop of $L_{\mathrm{EDC}}$ from $-5$ to $-25$ dB, multiplied by a factor of 3. Further, $T_{30}$ is the decay time predicted from a decrease in $L_{\mathrm{EDC}}$ from $-5$ to $-35$, multiplied by a factor of 2. Finally, LDT is the decay time with the limits of $-25$ and $-35$ dB in $L_{\mathrm{EDC}}$, multiplied by a factor of 6.

Figure 8 shows shapes of $L_{\mathrm{EDC}}$ determined at the previously assumed receiving point for the sound source located in subroom A (blue line) and subroom B (red line). The first observation is that for the source located in subroom A, changes in $L_{\mathrm{EDC}}$ are almost linear when $L_{\mathrm{EDC}}$ drops more than 15 dB, and the $L_{\mathrm{EDC}}$ curve has a clearly concave shape when the source is located in subroom B. The second observation is more important. Namely, the decay curves in Fig. 8 prove that moving the source from subroom A to subroom B causes significant reduction of decay times. This conclusion is supported by the data in Table 1,

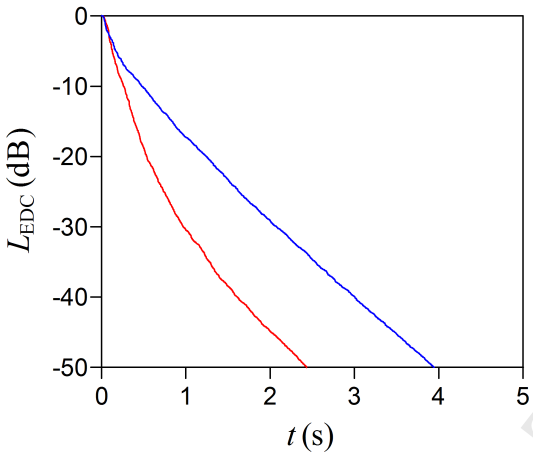


Figure 8: Shapes of $L_{\mathrm{EDC}}$ at receiving point for source located in subroom A (blue line) and subroom B (red line).

which presents the results of predicting the decay times from the decay curves in Fig. 8.

Table 1: Decay times EDT, $T_{10}$, $T_{20}$, $T_{30}$ and LDT determined from decay curves in Fig. 8.

| Source location | Decay times in seconds | | | | |
|---|---|---|---|---|---|
| | EDT | $T_{10}$ | $T_{20}$ | $T_{30}$ | LDT |
| subroom A | 2.97 | 4.11 | 4.53 | 4.87 | 5.59 |
| subroom B | 1.52 | 1.71 | 1.93 | 2.42 | 3.37 |

The data in Table 1 indicate that locating the source in subroom B causes an approximately twofold reduction of EDT and $T_{30}$, and also a more than twofold decrease in the decay times $T_{10}$ and $T_{20}$. It also follows from Fig. 8 that the concave nature of the decay curve is much greater for the source located in subroom B, and furthermore in this case there is no typical double-sloped energy decay because this decay is multi-sloped. The different shapes of the decay curves for the source located in subrooms A and B result from the influence of two factors on the sound decay process. The first of them is a different sound absorption on boundary surfaces because subroom A is highly reverberant, while walls of subroom B provide moderate sound damping. The second is the phenomenon of localization of eigenmodes, which in the considered system of coupled spaces manifests itself by the

concentration of eigenmode energy in subroom A or subroom B (Figs. 3(a)(c)(f)(h)).

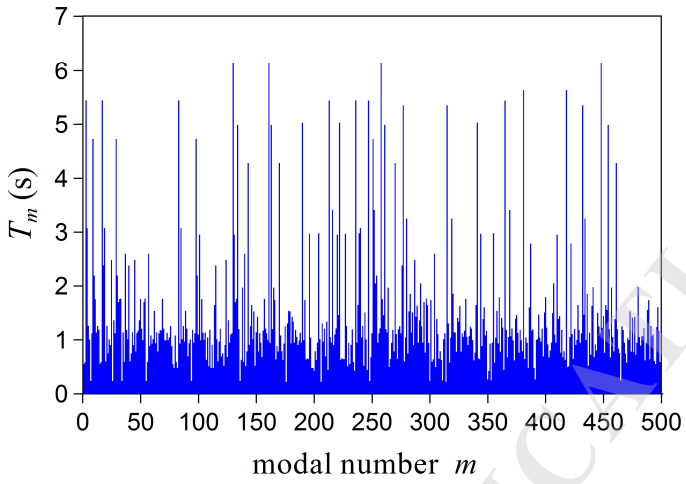


Figure 9: Modal reverberation time $T_m$ for first 500 eigenmodes.

The localization of eigenmodes is a consequence of the irregular distribution of the eigenfunctions $\Phi_m(\mathbf{r})$ in $(x, y)$ plane, hence, according to Eqs. (5) and (10), the parameter that unambiguously characterizes this phenomenon is the modal reverberation time $T_m$. In numerical study, 5450 eigenmodes were used, therefore, to clearly show the changes in $T_m$, in Fig. 9 the modal number $m$ was limited to 500. The calculation results presented in Fig. 9 are particularly interesting because they show how a different sound absorption in subrooms can affect the sound decay process in the considered two-room coupled system. It turns out that the significant difference in sound absorption in subrooms results in a wide range of modal decay time values. Indeed, the data in Fig. 9 show that for modes strongly localized in subroom A, the modal reverberation time $T_m$ is even above 6 seconds, while for modes strongly localized in subroom B the value of $T_m$ is even below 0.3 seconds.

Based on the foregoing analysis, the results in Fig. 8 can be explained as follows. If the sound source is located in subroom A, the response of the room system to this excitation is dominated by slowly decaying modes that are localized in this subroom. Therefore, decay times increase from about 3 seconds in the early decay stage to as much as 5.59 seconds in the late decay stage, as may be seen from the data in Table 1. In contrast, when the source is located in subroom B, non-localized modes with shorter modal reverberation time are excited in subroom A in the early stage of sound decay, so the EDT is 1.57 seconds, which

is approximately half that for the source located in subroom A. The influence of modes localized in subroom A is, however, visible in the late decay stage, because the LDT reaches a value of 3.37 seconds.

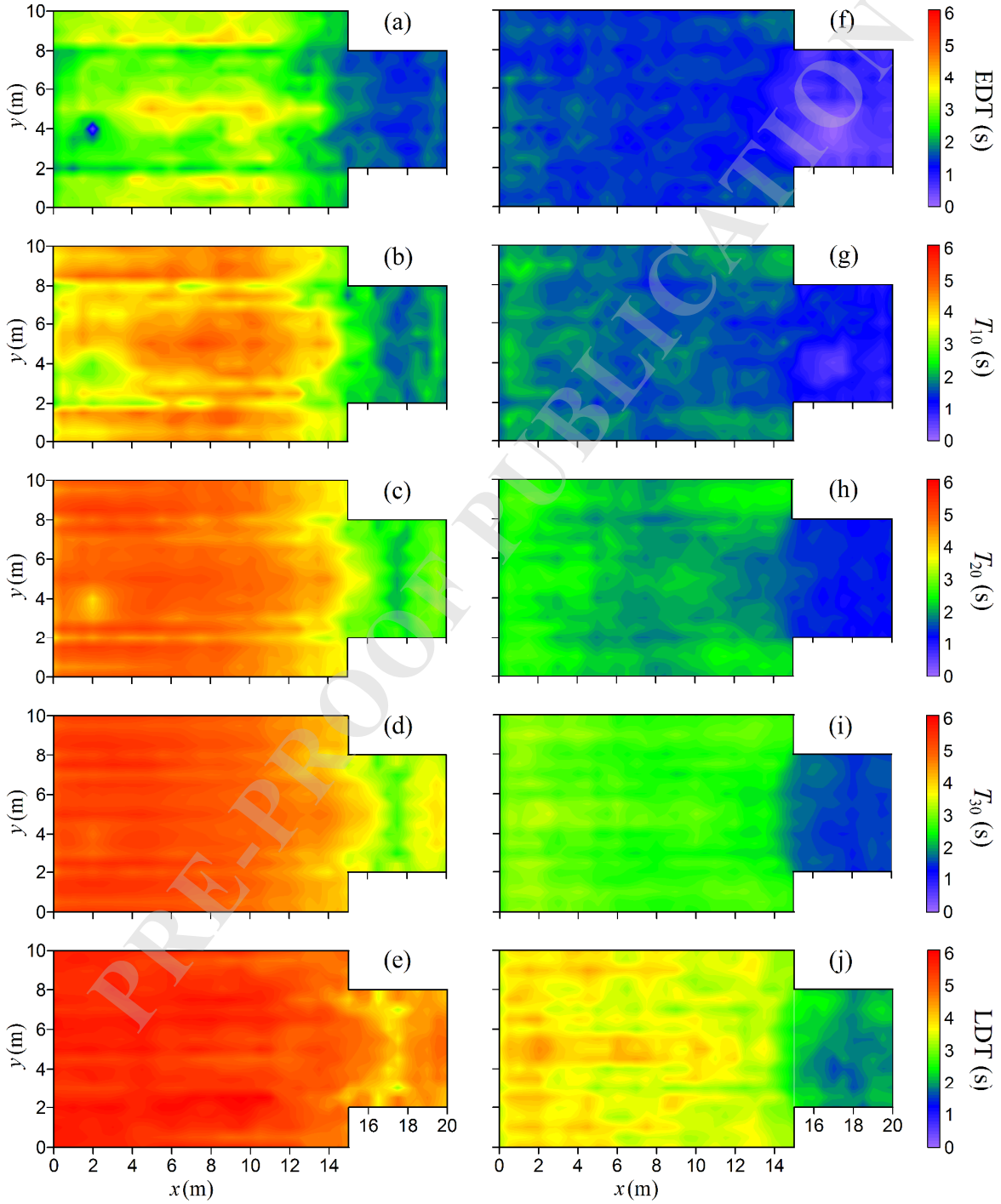


Figure 10: Distribution of decay times EDT, $T_{10}$, $T_{20}$, $T_{30}$ and LDT on observation plane for source located in: (a)–(e) subroom A and (f)–(j) subroom B.

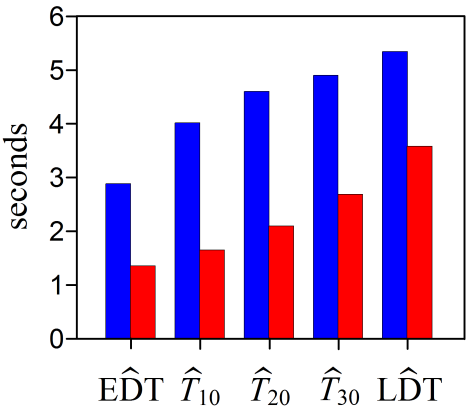


Figure 11: Mean decay times $\widehat{\text{EDT}}$, $\widehat{T}_{10}$, $\widehat{T}_{20}$, $\widehat{T}_{30}$, $\widehat{\text{LDT}}$ on observation plane in subroom A for source located in subrooms A (blue bars) and subroom B (red bars).

An important conclusion arising from the above analysis is that, in the considered room system, the nature of sound decay at the receiving point located in subroom A can be significantly modified by changing the position of the source. To check whether this also holds true for other points, the distributions of all considered decay times in the observation plane were calculated. The obtained results in the form of colored contour maps are shown in Fig. 10. They confirm and simultaneously generalize the previous findings, as it follows from Fig. 10 that placing the source in subroom B causes a significant shortening of all decay times in the observation plane.

It can be seen from Fig. 10 that the decay times predicted in subroom A vary moderately. This fact allows to characterize the sound decay process in subroom A by the mean values of the decay times on the observation plane. Since calculations were carried out in a finite number of observation points, the mean decay times were determined using an arithmetic averaging. The results of calculating these quantities, labelled $\widehat{\text{EDT}}$, $\widehat{T}_{10}$, $\widehat{T}_{20}$, $\widehat{T}_{30}$ and $\widehat{\text{LDT}}$, are collated in Fig. 11 and illustrated by vertical bars. Similar to the data in Table 1, this figure shows that placing the source in subroom B leads to an approximately twofold reduction of $\widehat{\text{EDT}}$ and $\widehat{T}_{30}$, as well as a more than twofold decrease in $\widehat{T}_{10}$ and $\widehat{T}_{20}$. However, such significant reduction of $\widehat{\text{LDT}}$ is not observed, because slowly decaying modes localized in subroom A start to dominate in the late decay stage.

The calculation results in Fig. 10 were obtained when eigenmodes with the frequencies

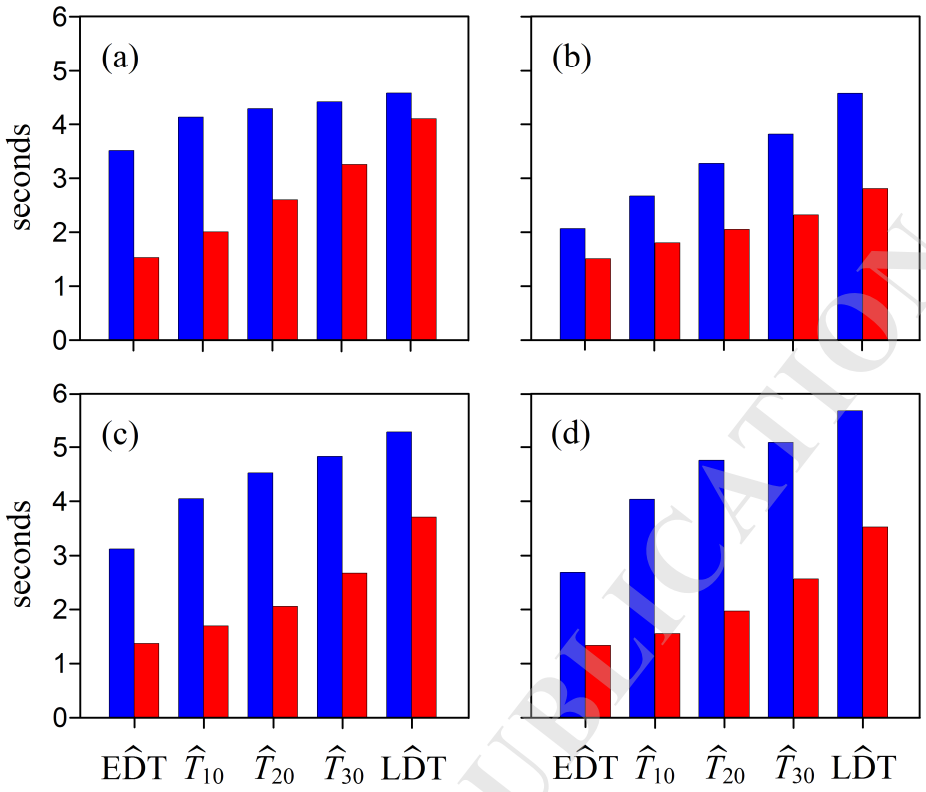


Figure 12: Mean decay times $\widehat{\mathrm{EDT}}$, $\widehat{T}_{10}$, $\widehat{T}_{20}$, $\widehat{T}_{30}$, $\widehat{\mathrm{LDT}}$ on observation plane in subroom A for octave bands: (a) 31.5 Hz, (b) 63 Hz, (c) 125 Hz, (d) 250 Hz. Results marked with blue and red bars correspond to source located in subrooms A and B, respectively.

$f_m$ up to 400 Hz were used to determine the RIR function (Eq. (11)). However, since in a low-frequency range the character of sound decay depends on frequency, it is equally important to predict the decay times in frequency bands such as octaves. In the developed theoretical model, a bandpass filtering of the RIR function can be realized by summing such components of the series in Eq. (11) for which $f_l < f_m < f_u$, where $f_l$ and $f_u$ are the lower and upper limits of octave bands. Then, using Eq. (16), $L_{\mathrm{EDC}}$ for particular octave band can be determined and by applying the linear regression to appropriate parts of $L_{\mathrm{EDC}}$, the decay times at observation points can be calculated, and then, from their values, the mean decay times on the observation plane lying in subroom A can be predicted.

Since the frequency range is limited to 400 Hz, the mean decay times were computed for octave bands with the center frequency of 31.5 Hz, 63 Hz, 125 Hz and 250 Hz. The calculation results are presented in Fig. 12. They prove that for octave bands with the center frequency

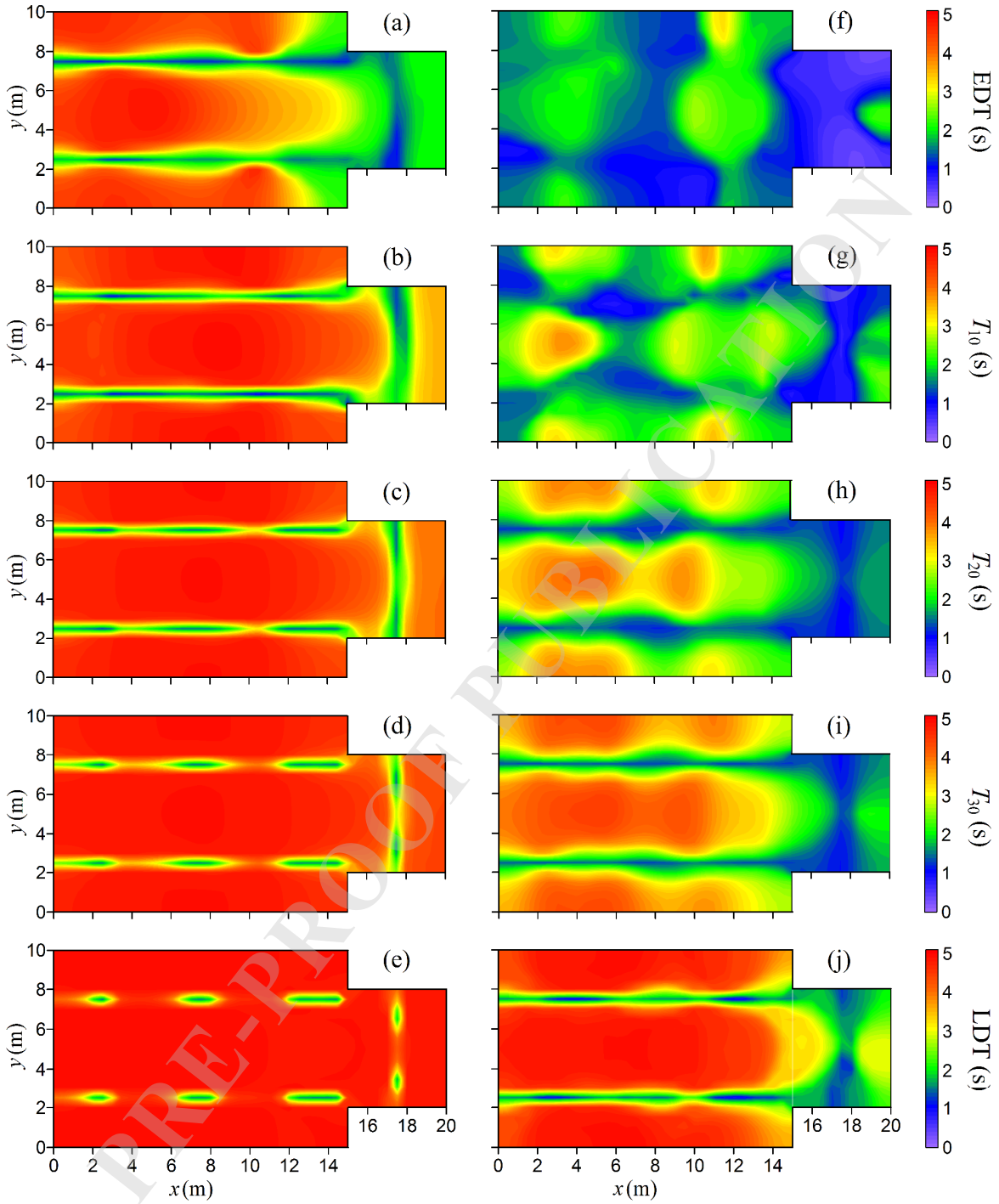


Figure 13: Distribution of decay times EDT, $T_{10}$, $T_{20}$, $T_{30}$, LDT on observation plane for octave band 31.5 Hz and source located in: (a)–(e) subroom A and (f)–(j) subroom B.

of 125 Hz and 250 Hz the mean decay times $\widehat{\text{EDT}}$, $\widehat{T}_{10}$, $\widehat{T}_{20}$, $\widehat{T}_{30}$ are approximately twice as small when the source is located in subroom B. These results are very similar to those

obtained for the frequency band up to 400 Hz (Fig. 11), and this is because in these octaves there is a large number of eigenmodes, 473 and 3312, respectively. Obviously, such a rule is not visible for octave bands with a center frequency of 31.5 Hz and 63 Hz, as the number of eigenmodes in these octaves is very small, i.e. 11 and 69, respectively. This is particularly true for the first octave, which contains a strongly localized eigenmode with the frequency of 34.5 Hz and the modal reverberation time of 4.9 seconds. The shape of the eigenfunction $\Psi_\kappa$ for this eigenmode is shown in Fig. 3(a). As can be seen in Fig. 13, this eigenmode dominates the sound decay process when the source is located in subroom A. Moreover, when the source is placed in subroom B, this mode strongly influences the sound decay process in the late decay stage.

## 4. Summary and conclusions

Sound decay is a fundamental and easily noticeable acoustic feature of enclosed spaces, hence one of the basic goals of room acoustics is to assess sound decay times based on the reverberant sound field in enclosed spaces. In this paper, the sound decay in the system of two connected enclosed spaces with a different sound absorption on boundary surfaces was analyzed. The theoretical model was based on the modal expansion of sound pressure, since at low frequencies acoustic modes excited in enclosed spaces can have a significant influence on the sound decay process. Two types of reverberant responses of the system were examined. In the first case, the system was driven by a harmonic point source, and the sound decay process began immediately after the source was turned off. In the second case, the reverberant response of the system was initiated by the Dirac delta time impulse emitted by a point source.

Using the presented theoretical model, numerical simulations of the sound decay process was performed for a system of two connected rectangular subrooms of the same height. The larger subroom marked A was highly reverberant, while the smaller subroom marked B had walls that provided moderate sound damping. The eigenfunctions and eigenfrequencies of this system were determined using the finite element method. The obtained calculation results showed that after switching off the harmonic source, the sound decay curves usually have an irregular shape. This is because the sound decay process, which has been shown

to strongly depend on both the source frequency and the source location, is generally non-exponential. Only when this process is dominated by the eigenmode localized in subroom A, an exponential sound decay was observed.

Another method used to evaluate the reverberant properties of the analyzed two-room coupled system was based on the reverse-time integration of RIR. By applying this method, smooth energy decay curves were obtained and based of their slope, the decay times EDT, $T_{10}$, $T_{20}$, $T_{30}$ and LDT were determined. Calculation results demonstrated that a different sound absorption in subrooms significantly impacts the sound decay process because it results in a wide range of modal decay time values. This is because these values are large for eigenmodes strongly localized in subroom A and very small for eigenmodes strongly localized in subroom B. Thus, the system under consideration has an interesting feature that is the result of the phenomenon of localization of eigenmodes. Namely, if the source is located in subroom A, the sound decay process in subroom A is dominated by slowly decaying modes that are strongly localized in this subroom. However, when the source is located in subroom B, non-localized modes with shorter modal reverberation time are excited in subroom A in the early stage of sound decay. Therefore, as calculation results showed, in this case the decay times in subroom A are approximately half that for the source located in subroom A. Obviously, this regularity does not occur in the late stage of sound decay, because in this stage the modes localized in subroom A start to influence the sound decay.

### Fundings

This research did not receive any specific grant from funding agencies in the public, commercial, or not-for-profit sectors.

### Conflict of interest

The authors declare that they have no known competing financial interests or personal relationships that could have appeared to influence the work reported in this paper.





## References

1. Bradley D.T., Wang L.M. (2007), Comparison of measured and computer-modeled objective parameters for an existing coupled volume concert hall, *Building Acoustics*,

**14**(2): 79–90, https://doi.org/10.1260/135101007781448028.

2. Bradley D.T., Wang L.M. (2009), Quantifying the double slope effect in coupled volume room systems, *Building Acoustics*, **16**(2): 105–123, https://doi.org/10.1260/135101009788913275.

3. Bradley D.T., Wang L.M. (2010), Optimum absorption and aperture parameters for realistic coupled volume spaces determined from computational analysis and subjective testing results, *Journal of the Acoustical Society of America*, **127**(1): 223–232, https://doi.org/10.1121/1.3268604.

4. Collins P.J. (2006), Differential and Integral Equations, Oxford University Press, New York.

5. Das O., Abel J.S. (2021), Grouped feedback delay networks for modeling of coupled spaces, *Journal of the Audio Engineering Society*, **69**(7/8): 486–496, https://doi.org/10.17743/jaes.2021.0026.

6. Ermann M., Johnson M. (2005), Exposure and materiality of the secondary room and its impact on the impulse response of coupled-volume concert halls, *Journal of Sound and Vibration*, **284**(3-5): 915–931, https://doi.org/10.1016/j.jsv.2004.07.030.

7. Girón S., Álvarez-Morales L., Zamarreño T. (2017), Church acoustics: A state-of-the-art review after several decades of research, *Journal of Sound and Vibration*, **411**: 378–408, https://doi.org/10.1016/j.jsv.2017.09.015.

8. Jasa T., Xiang N. (2009), Efficient estimation of decay parameters in acoustically coupled-spaces using slice sampling, *Journal of the Acoustical Society of America*, **126**(3): 1269–1279, https://doi.org/10.1121/1.3168507.

9. Kak S. (1970), The discrete Hilbert transform, *Proceedings of the IEEE*, **58**(4): 585–586, https://doi.org/10.1109/PROC.1970.7696.

10. Kinsler L.E., Frey A.R., Coppens A.B., Sander J.V. (2000), Fundamentals of Acoustics, 4th ed., John Wiley & Sons, New York.

11. Kuttruff H. (2017), Room Acoustics, 6th ed., CRC Press, New York.

12. Luizard P., Katz B.F.G. (2014a), Investigation of the effective aperture area of sliding and hinged doors between coupled spaces, *Journal of the Acoustical Society of America*, **136**(2): 1269–1279, http://dx.doi.org/10.1121/1.4890202.

13. Luizard P., Polack J-D., Katz B.F.G. (2014b), Sound energy decay in coupled spaces using a parametric analytical solution of a diffusion equation, *Journal of the Acoustical Society of America*, **135**(5): 2765–2776, http://dx.doi.org/10.1121/1.4870706.

14. Luizard P., Katz B.F.G., Guastavino C. (2015), Perceived suitability of reverberation in large coupled volume concert halls, *Psychomusicology: Music, Mind, and Brain*, **25**(3): 317–325, https://doi.org/10.1037/pmu0000109.

15. Martellotta F. (2016), Understanding the acoustics of Papal Basilicas in Rome by means of a coupled-volumes approach, *Journal of Sound and Vibration*, **382**: 413–427, http://dx.doi.org/10.1016/j.jsv.2016.07.007.

16. Meissner M. (2009), Spectral characteristics and localization of modes in acoustically coupled enclosures, *Acta Acustica united with Acustica*, **95**(2): 300–305, https://doi.org/10.3813/AAA.918152.

17. Meissner M. (2010), Simulation of acoustical properties of coupled rooms using numerical technique based on modal expansion, *Acta Physica Polonica A*, **118**(1): 123–127, https://doi.org/10.12693/APhysPolA.118.123.

18. Meissner M. (2012), Acoustic energy density distribution and sound intensity vector field inside coupled spaces, *Journal of the Acoustical Society of America*, **132**(1): 228–238, https://doi.org/10.1121/1.4726030.

19. Meissner M., Wiśniewski K. (2019), Influence of room modes on low-frequency transients: theoretical modeling and numerical predictions, *Journal of Sound and Vibration*, **448**: 19–33, https://doi.org/10.1016/j.jsv.2019.02.012.

20. Meissner M., Wiśniewski K. (2020), Investigation of damping effects on low-frequency steady-state acoustical behaviour of coupled spaces, *Royal Society Open Science*, **7**(8): 200514, https://doi.org/10.1098/rsos.200514.

21. Nijs L., Jansens G., Vermeir G., van der Voorden M. (2002), Absorbing surfaces in ray-tracing programs for coupled spaces, *Applied Acoustics*, **63**(6): 611–626, https://doi.org/10.1016/S0003-682X(01)00063-9.

22. Paris E.T. (1928), On the coefficient of sound-absorption measured by the reverberation method, *The London, Edinburgh, and Dublin Philosophical Magazine and Journal of Science*, **5**(29): 489–497, https://doi.org/10.1080/14786440308565092.

23. Schroeder M.R. (1965), New method of measuring reverberation time, *Journal of the Acoustical Society of America*, **37**(6): 409–412, https://doi.org/10.1121/1.1909343.

24. Schroeder M.R. (1996), The "Schroeder frequency" revisited, *Journal of the Acoustical Society of America*, **99**(5): 3240–3241, https://doi.org/10.1121/1.414868.

25. Shi S., Jin G., Xiao B., Liu Z. (2018), Acoustic modeling and eigenanalysis of coupled rooms with a transparent coupling aperture of variable size, *Journal of Sound and Vibration*, **419**: 352–366, https://doi.org/10.1016/j.jsv.2018.01.024.

26. Summers J.E., Torres R.R., Shimizu Y. (2004), Statistical-acoustics models of energy decay in systems of coupled rooms and their relation to geometrical acoustics, *Journal of the Acoustical Society of America*, **116**(2): 958–969, https://doi.org/10.1121/1.1763974.

27. Summers J.E., Torres R.R., Shimizu Y., Dalenbäk B-I.L. (2005), Adapting a randomized beam-axis-tracing algorithm to modeling of coupled rooms via late-part ray tracing, *Journal of the Acoustical Society of America*, **118**(3): 1491–1502, https://doi.org/10.1121/1.2000772.

28. Summers J.E. (2012), Accounting for delay of energy transfer between coupled rooms in statistical-acoustics models of reverberant-energy decay, *Journal of the Acoustical Society of America*, **132**(2), 129–134, https://doi.org/10.1121/1.4734591.

29. Sü Gül Z., Odabaş E., Xiang N., Çalışcan M. (2019), Diffusion equation modeling for sound energy flow analysis in multi domain structures, *Journal of the Acoustical Society of America*, **145**(4): 2703–2717, https://doi.org/10.1121/1.5095877.

30. Sü Gül Z. (2021), Exploration of room acoustics coupling in Hagia Sophia of Istanbul for its different states, *Journal of the Acoustical Society of America*, **149**(1): 320–339, https://doi.org/10.1121/10.0002971.

31. Thydal T., Pind F., Jeong C.H., Engsig-Karup A.P. (2021), Experimental validation and uncertainty quantification in wave-based computational room acoustics, *Applied Acoustics*, **178**: 107939, https://doi.org/10.1016/j.apacoust.2021.107939.

32. Vorländer M. (2020), Auralization: Fundamentals of Acoustics, Modelling, Simulation, Algorithms and Acoustic Virtual Reality, 2nd ed., Springer, Berlin.

33. Xiang N., Jing Y., Bockman A.C. (2009), Investigation of acoustically coupled enclosures using a diffusion-equation model, *Journal of the Acoustical Society of America*, **126**(3): 1187–1198, https://doi.org/10.1121/1.3168507.

34. Xiang N., Goggans P., Jasa T., Robinson P. (2011), Bayesian characterization of multiple-slope sound energy decays in coupled-volume systems, *Journal of the Acoustical Society of America*, **129**(2): 741–752, https://doi.org/10.1121/1.3518773.